ELectronics EXpress

LETTER

IEICE Electronics Express, Vol.13, No.20, 1–8

Research on cross section of UHF radio wave scattering from surface waves on water

Yan Tu[a)], **Biyang Wen**[b)], **Ke Li, and Jing Yang**

Electronic Information School, Wuhan University,

Wuhan, Hubei Province, 430072, China

a) *tuyan@whu.edu.cn*

b) *rspl@whu.edu.cn*

Abstract: Bragg scattering mechanism has been probed by a fully digital ultra-high-frequency (UHF) radar system. The system is based on studies of UHF radio wave (340 MHz) scattering from small-amplitude water waves. First-order radar cross section Doppler spectra have been measured. Comparing them with theoretical models, good agreement has been found. The amplitude ratio (dB) of the cross section between incident and reflected waves is 14.7 dB, and its deviation is 0.68%. The expectation of the normalized Doppler frequency shift of first-order peaks is 0.9850, and the deviation is 1.5%.

Keywords: UHF radar, Bragg scattering, radar cross section

Classification: Microwave and millimeter-wave devices, circuits, and modules

References

[1] D. D. Crombie: "Doppler spectrum of sea echo at 13.56 Mc./s," Nature **175** (1955) 681 (DOI: 10.1038/175681a0).

[2] D. Barrick: "First-order theory and analysis of MF/HF/VHF scatter from the sea," IEEE Trans. Antennas Propag. **20** (1972) 2 (DOI: 10.1109/TAP.1972.1140123).

[3] D. Barrick: "Remote sensing of sea state by radar," Int. Conf. Eng. in Ocean Environment (1972) 186 (DOI: 10.1109/OCEANS.1972.1161190).

[4] B. Lipa: "Derivation of directional ocean-wave spectra by integral inversion of second-order radar echoes," Radio Sci. **12** (1977) 425 (DOI: 10.1029/RS012i003p00425).

[5] B. Lipa, *et al.*: "Directional wave information from the SeaSonde," IEEE J. Oceanic Eng. **30** (2005) 221 (DOI: 10.1109/JOE.2004.839929).

[6] A. Abou-Taleb and D. Cooper: "Microwave scattering by surface waves on water," IEEE J. Oceanic Eng. **11** (1986) 316 (DOI: 10.1109/JOE.1986.1145171).

[7] E. D. R. Shearman: "High spatial resolution observations of radar scattering from a wave tank," IEE Colloquium on Interaction of Radiowaves with the Sea Surface, IET (1990) 4/1.

[8] H. Li, *et al.*: "High-resolution Doppler radar observation of scattering from waves in laboratory wave-tanks," ICAP 89 (1989) 312.

[9] P. H. Y. Lee, *et al.*: "Experiments on Bragg and non-Bragg scattering using single-frequency and chirped radars," Radio Sci. **32** (1997) 1725 (DOI: 10.

DOI: 10.1587/elex.13.20160898
Received September 9, 2016
Accepted September 20, 2016
Publicized October 7, 2016
Copyedited October 25, 2016

1029/97RS01399).
[10] S. A. Ermakov, *et al.*: "Radar scattering on gravity-capillary waves: Laboratory investigation," Izv., Atmos. Ocean. Phys. **43** (2007) 243 (DOI: 10.1134/S0001433807020119).
[11] K. Li, *et al.*: "A novel UHF radar system design for river dynamics monitoring," IEICE Electron. Express **12** (2015) 20141074 (DOI: 10.1587/elex.12.20141074).
[12] G. Neumann, *et al.*: *Principles of Physical Oceanography* (Prentice-Hall, cop., Englewood Cliffs, 1966).
[13] Y. Goda, *et al.*: "Estimation of incident and reflected waves in random wave experiments," Proc. 15th Coastal Engrg. Conf. **1** (1976) 2156.

1 Introduction

Since Crombie first interpreted the dominant components of backscattered sea echoes in the high-frequency (HF) band with Bragg resonance theory [1], HF radar has been strongly associated with the remote sensing of sea surface states. Barrick [2, 3] deduced first-order radar cross sections and second-order radar cross sections quantitatively via perturbation results. These cross sections can be used to extract physical states of an ocean surface such as current vectors, wind fields and waveheight fields. Therefore, intensive investigations have been conducted, and many inversion methods have been proposed during the past several decades. Lipa [4] proposed an inversion method which assumed that there is no correlation between wave direction and wave frequency. And she [5] described two method to obtain wave information from SeaSonde (a compact HF radar system) data, the first, integral inversion which provided detailed wave information under a somewhat restricted set of conditions. The second involved fitting with a model of the ocean wave spectrum. However, because of the complex mechanism underlying the interaction of electromagnetic waves and the sea surface, the above methods cannot always be applied due to certain assumptions and the constraints on which they are based. Controlled variable experiments are the optimal choice for exploring relationships between radar cross sections and ocean state conditions. For instance, a single frequency wave can be generated artificially and probed in a controlled variable experiment. But wavelength that HF radar can probe range from several meters to tens of meters; in other words, the conditions are out of control range of the experimenter. Hence, scaled experiments can be considered to explore the relationship.

A number of in-depth studies on sea echos using scaled experiments have been conducted in recent years. Cooper [6, 7, 8] conducted a series of measuring about first- and second-order backscatter Doppler spectra based on a microwave model, and the results were in accord with theoretical models. Lee et al. [9] conducted a series of laboratory experiments to distinguish Bragg and non-Bragg scattering using different polarizations. Ermakov [10] studied the mechanism of the Bragg resonance scattering of microwaves using gravity-capillary waves. Most studies have focused on capillary waves using microwave scattering, but ocean surface state sensing with HF ground wave radar probes deep-water gravity waves. UHF radar operates in the frequency range between microwave and high frequencies,

DOI: 10.1587/elex.13.20160898
Received September 9, 2016
Accepted September 20, 2016
Publicized October 7, 2016
Copyedited October 25, 2016

with wavelengths ranging from 0.1 m to 1 m. It can be concluded that the corresponding water waves in a flume could be deep-water gravity waves. Another observation is that UHF radio waves exhibit less energy attenuation than do microwaves in the communication process. It accepts a wider range of water wave periods. Consequently, UHF radar is preferred in the study of the mechanism of Bragg scattering.

This letter measures first-order Bragg scattering using a fully digital UHF (340 MHz) radar system, which has not been used in previous flume experiments. Section 2 briefly explains Barrick's formulas. Section 3 describes the hardware composition of the radar system and corresponding waveform parameter design in the flume experiment. In Section 4, data on radar echo are analyzed theoretically and statistically. Section 5 concludes this letter.

2 First-order scattering theory

The Doppler frequency shift of radio waves reflected from the sea surface at 13.56 MHz was recorded by Crombie in 1955 [1]. These records show that the frequency of the principal component is surprisingly constant at approximately 0.38 Hz, irrespective of wind conditions and the state of the sea. Analogous to diffraction gratings, one tentative explanation is that the waves traveling radially to the antenna with a wavelength $L = \lambda/2$, with λ being the radio wavelength, will generate Bragg scattering, also called first-order scattering. Therefore, the Doppler shift Δf can be derived as follows:

Under deep water conditions, due to the effects of gravity, the relationship between the wavelength L and wave phase velocity V_p is as follows [1]:

$$V_p = \sqrt{\frac{gL}{2\pi}} \tag{1}$$

where g is the acceleration of gravity. When the sea wavelength $L = \lambda/2$, the Doppler shift f_d will be expressed as

$$f_d = \frac{2V_p}{\lambda} = \sqrt{\frac{g}{\pi\lambda}} \tag{2}$$

The equation for the first-order radar spectral cross section in deep water without sea surface current proposed by Barrick is as follows [2]:

$$\sigma^{(1)}(\omega, \phi) = 2^6 \pi k_0^4 \sum_{m=\pm 1} S(-2m\tilde{k}_0)\delta(\omega - m\omega_B) \tag{3}$$

where ω is the Doppler shift, k_0 is the radar wavenumber, $m = \pm 1$ denotes the sign of the Doppler shift, $S(\cdot)$ is the directional waveheight spectrum, and ω_B is the Bragg angular frequency caused by the gravity wave phase velocity, which is given by

$$\omega_B = \sqrt{2k_0 g} \tag{4}$$

The Bragg frequency f_B is

$$f_B = \omega_B/(2\pi) \tag{5}$$

The equation indicates that the first-order radar cross section is a pulse function under the Bragg frequency ω_B in ideal cases. In other words, a wave with fre-

DOI: 10.1587/elex.13.20160898
Received September 9, 2016
Accepted September 20, 2016
Publicized October 7, 2016
Copyedited October 25, 2016

quency $\omega = \omega_B$ traveling radially toward and from antennas will cause Bragg resonance [2].

3 Description of flume experiment

To simulate the Bragg scattering from sea waves of radio waves, the experiment was based on a fully digital UHF radar system and multifunction wave flume [11].

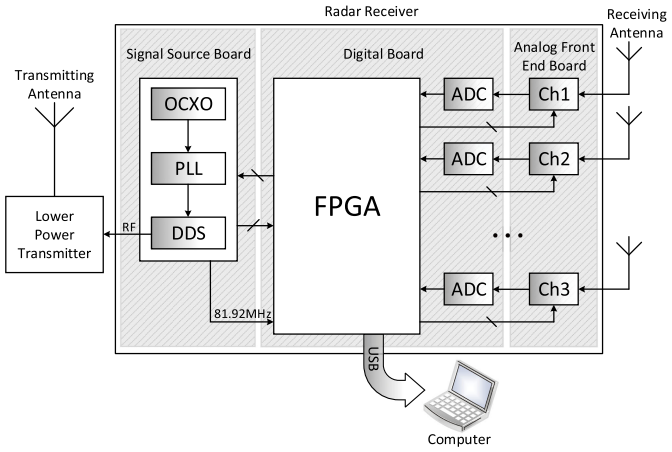

Fig. 1. Fully digital UHF radar system.

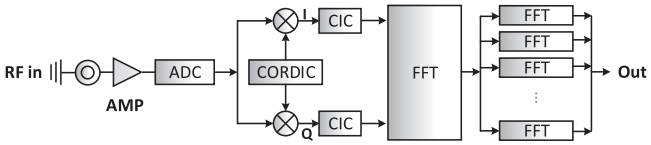

Fig. 2. Fully digital UHF radar system and signal processing.

As demonstrated in Fig. 1, the UHF radar system consists of three components: a Signal Source Board, a Digital Board, and an Analog Front-End Board.

In the signal source board, a novel model of "DSPLL+DDS" is applied to realize accuracy control of the signal phase and frequency under implementation of the digital board, which inputs waveform parameters to the radar system. The digital board consists of six ADCs, one FPGA, one clock buffer and one universal serial bus (USB). The analog front-end board includes six identical structure channels, each channel containing two high-speed RF switches, three band-pass filters, and two wide-band amplifiers.

The signal processing of this system is achieved using a multi-channel coherent system. The flow diagram of the signal processing is shown in Fig. 2. This processing includes AD sampling, quadrature downconversion based on CORDIC, sample rate conversion, etc.

This radar system adopts the Linear Frequency Modulated Interrupted Continuous Waveform (LFMICW) mechanism and operates at 340 MHz, which depends on the presence of 44-cm-wavelength waves. The sweep bandwidth is $B = 15$ MHz, and the sweep period is $T_s = 0.043$ s; therefore, the range resolution is $\Delta R = c/2B = 10$ m. Because the length of the flume is short, the maximum

DOI: 10.1587/elex.13.20160898
Received September 9, 2016
Accepted September 20, 2016
Publicized October 7, 2016
Copyedited October 25, 2016

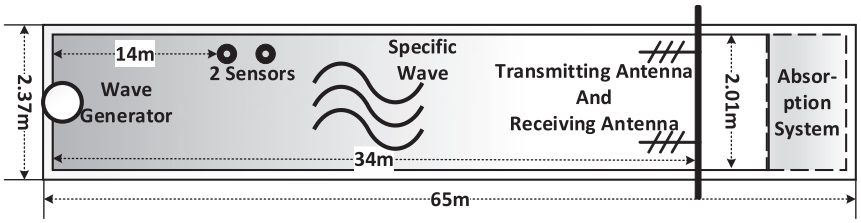

Fig. 3. The overall structure of the experimental flume. Two antennas are 1 m above the water surface.

detection length is 300 m. The pulse repetition period is set to $q = 5.2368\,\mu s$. For receiving echo signals among the whole flume, there is no range blind in the parameter design. There are $N = 256$ sweep periods in one coherent integration period; therefore, the coherent integration time is $t = N \times T_s = 11.08\,s$ per dataset. The Doppler resolution is $\Delta f = 1/t = 0.09\,Hz$, with a velocity resolution $\Delta v = \Delta f \lambda/2 = 0.04\,m/s$.

The multifunction wave flume was provided by the State Key Laboratory of Coastal and Offshore Engineering of Dalian University of Technology. The overall structure of the experimental flume is given in Fig. 3. The distance between two sensors is 34.7 cm. Each single-frequency plane water wave is generated by a multi-functional wave generator located on one side of the flume, and the absorption system lies on the other side of the flume to absorb most of the reflected waves. Two pressure sensors are adopted to monitor the water waveform and for comparison with radar data as a reference.

This UHF radar system works at $f_0 = 340\,MHz$, and the radio wavelength is $\lambda = c/f_0 = 0.88\,m$. Hence, the water wave period producing first-order Bragg scattering is [12]

$$T = \sqrt{\frac{2\pi L}{g} \Big/ \tanh\frac{2\pi d}{L}} \approx 0.5371\,s \tag{6}$$

where $L = (1/2)\lambda = 0.44\,m$ is the wavelength, and $d = 0.8\,m$ is the working depth of the wave flume.

According to (4) and (5), Bragg angular frequency caused by the gravity wave phase velocity $\omega_B = \sqrt{2k_0 g} = 11.81\,rad$, and the Bragg frequency $f_B = \omega_B/(2\pi) = 1.88\,Hz$.

With increasing wave steepness $\alpha = H/L$, where H is the waveheight, a wave will be broken until the steepness reaches a threshold. It is important to determine whether the wave has been broken, and many researchers have proposed different bases for such a determination; however, an agreement has yet to be reached. Generally, it is suggested that the threshold of the steepness should be $\alpha_b = 0.14$ in deep waters. In this flume experiment, the water wavelength is $L = 0.44\,m$, and the theoretical maximum water waveheight is $H = 0.062\,m$ from the threshold of the steepness. However, a stable wave cannot be maintained when the waveheight increases to $H = 0.03\,m$ in this flume. In addition, the wave generator will not perform effectively when the water waveheight is too small. Considering these restrictions, the water waveheight should be chosen as $H = 0.01\,m$. The power of the reflected waves can be extracted using two sensors with different phases [13].

DOI: 10.1587/elex.13.20160898
Received September 9, 2016
Accepted September 20, 2016
Publicized October 7, 2016
Copyedited October 25, 2016

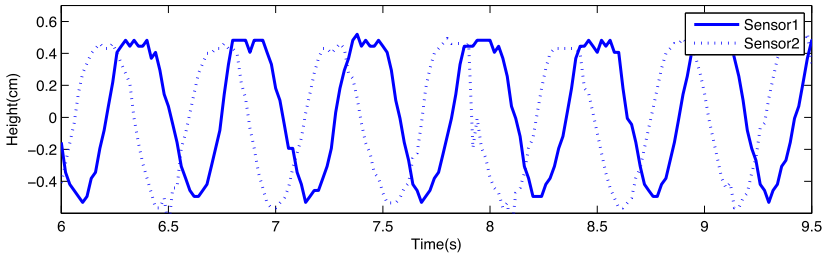

Fig. 4. The wave profile recorded by two sensors.

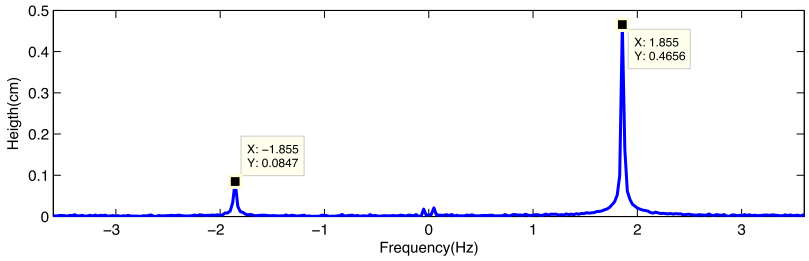

Fig. 5. The spectrum of the water wave after pretreatment. The positive frequency represents the power of the waves traveling toward the antennas, and the negative frequency represents the power of the reflected waves.

The wave profile of these water waves gathered by the pressure sensor is shown in Fig. 4, and the corresponding spectrum is exhibited in Fig. 5.

4 Analysis

Natural ocean surfaces contain waves with a variety of different directions and wavelengths. In contrast, in a laboratory test, there is a single-wavelength wave in the flume traveling toward the antennas. Thus, there is no second-order interaction between waves traveling in two different directions, and the first-order peak is the pulse function, whose value depends on the point of frequency $\omega = \omega_B$ only.

For a single-frequency water wave, the energy spectrum is given by

$$S(\omega) = \frac{1}{2}a^2 \tag{7}$$

where a is the amplitude of the single-frequency water wave.

According to (3), the first-order cross section can be represented by

$$\sigma^{(1)}(\omega, \phi) = 2^5 \pi k_0^4 a^2 \delta(\omega - \omega_B) \tag{8}$$

(8) demonstrates that the size of the first-order peak relates to the amplitude of the single-frequency water wave, and the location of the peak is the frequency of the water wave.

In this experiment, the assumption is that water waves travel only in the direction toward the antennas, as expected. However, for an unperfect absorption system using a sponge layer, there is a receding spectral component in the spectrum, and this component is produced by a reflected water wave, as shown in Fig. 5. The amplitude ratio (dB) of the cross section between incident and reflected waves in Fig. 5 is

DOI: 10.1587/elex.13.20160898
Received September 9, 2016
Accepted September 20, 2016
Publicized October 7, 2016
Copyedited October 25, 2016

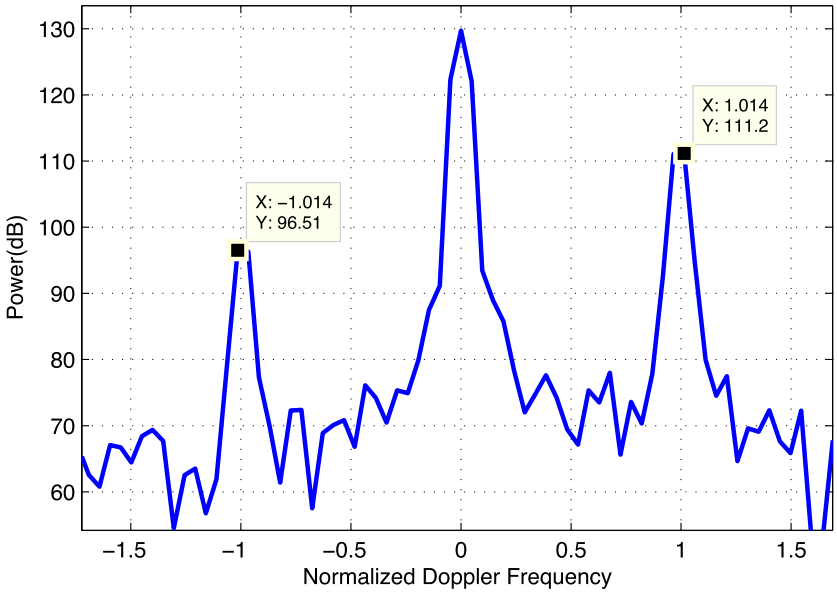

Fig. 6. The Doppler spectrum normalized by Bragg frequency $f_B = \omega_B/2\pi = 1.88\,\text{Hz}$.

$$A = 10lg\left(\frac{\sigma_I}{\sigma_r}\right) = 20lg\left(\frac{a_I}{a_R}\right) = 14.8\,\text{dB} \tag{9}$$

where $a_I = 0.4656\,\text{cm}$ and $a_R = 0.0847\,\text{cm}$ are the amplitudes of the incident and reflected waves and σ_I and σ_R are the cross sections of the waves. In Fig. 6, the right-hand peak represents the spectral line resulting from the water waves traveling toward the antennas, and the left-hand peak indicates the spectral line resulting from reflection. The difference between the two peaks is

$$\Delta = 111.2\,\text{dB} - 96.51\,\text{dB} = 14.7\,\text{dB} \tag{10}$$

The deviation is

$$\eta = \frac{14.8\,\text{dB} - 14.7\,\text{dB}}{14.8\,\text{dB}} = 0.68\% \tag{11}$$

The result is consistent with the actual situation based on sensor data.

As (8) shows, the first-order radar cross section $\sigma^{(1)}$ is proportional to the square of the amplitude of the single-frequency water wave a^2. Thus, the amplitude of the radar echo increased along with the water waves from generation to the target height, as demonstrated in Fig. 7. Once the water waves reached their target height, the amplitude of the radar echo was stable at approximately 105 dB (relative value).

The coherent integration time is $t = N \times T_s = 11.08\,\text{s}$ per dataset under the designed radar parameters. The water waveform in the flume changed so rapidly that radar echo cannot reflect the instantaneous form of the water wave in 11 s. Hence, 64 sweep pulses have been chosen for the coherent integration in the statistical analysis. The coherent integration time is $t = N \times T_s = 2.75\,\text{s}$.

In the ideal case, the normalized Doppler frequency shift of the first-order cross section would be simply $f_D = 1$. However, because the normalized Doppler frequency resolution is $\Delta f_N = \Delta f/f_B = 0.0454$, the normalized Doppler frequency shift $f_D = 1$ cannot be reached. This frequency can be either 0.9663 or 1.0146, which are nearby $f_D = 1$. Considering the first-order cross section of each

DOI: 10.1587/elex.13.20160898
Received September 9, 2016
Accepted September 20, 2016
Publicized October 7, 2016
Copyedited October 25, 2016

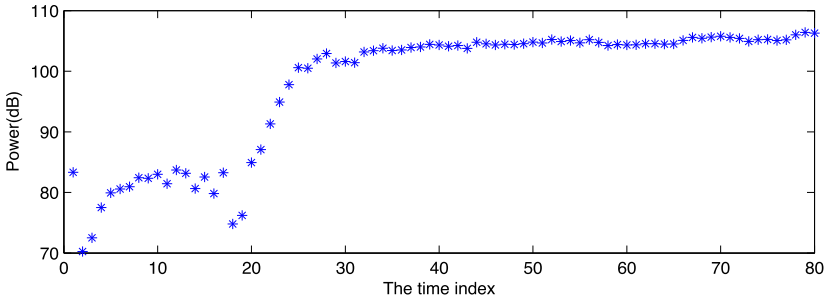

Fig. 7. The amplitude range of the first-order peak from when the water wave is just generated to when the water wave is stable. Each time index represents one coherent integration time, which equals 2.75 s. The ordinate represents the amplitude of the first-order peak.

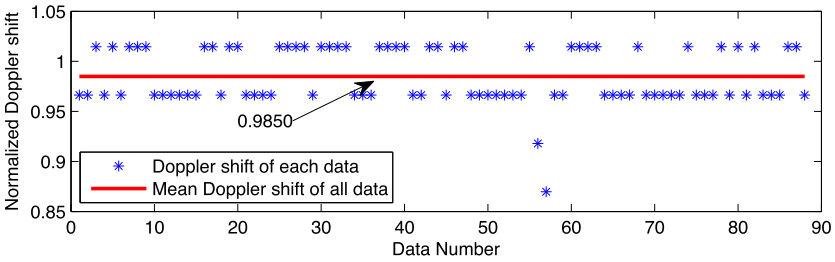

Fig. 8. Distribution of the Doppler shift of first-order peaks.

dataset, the distribution of the normalized Doppler frequency shift is shown in Fig. 8. The expectation of the Doppler frequency shift is

$$E_{f_D} = \frac{1}{n}\sum_{i}^{n} f_{Di} = 0.9850 \tag{12}$$

The deviation is $\eta = 1.5\%$, and the variance is $\delta^2 = 0.0278$.

5 Conclusions

The results obtained from the scaled experiment in the flume have verified the correction of the existing first-order scattering theory of Barrick. The first-order peak is located at the predicted position given by the theory of Barrick. Because of the limitations of the flume, directed waves could not be generated, and the verification of the second-order spectral components of two waves with different wave vectors will be achieved in future work. A water wave at the Bragg frequency in a flume has a relatively small waveheight. Thus, accurate measurements could not be easily obtained for analysis.

Acknowledgments

This research was supported by National Natural Science Foundation of China (Grant No. 61371063 and No. 61072086). The authors would like to acknowledge the support provided by the State Key Laboratory of Coastal and Offshore Engineering of Dalian University of Technology and the editors and the anonymous reviewers for their comments and suggestions, which were very helpful for improving the manuscript.

DOI: 10.1587/elex.13.20160898
Received September 9, 2016
Accepted September 20, 2016
Publicized October 7, 2016
Copyedited October 25, 2016